Achieving exceptionally high luminescence quantum efficiency by immobilizing an AIE molecular chromophore into a metal-organic framework

Zhichao Hu,[a] Guangxi Huang,[b] William P. Lustig,[a] Fangming Wang,[a,c] Hao Wang, [a] Simon J. Teat,[d] Debasis Banerjee,[a] Deqing Zhang,[b] and Jing Li*,[a]

[a] Department of Chemistry and Chemical Biology, Rutgers University, 610 Taylor Road, Piscataway NJ 08854, USA

[b] Beijing National Laboratory for Molecular Sciences, CAS Key Laboratory of Organic Solids, Institute of Chemistry, Chinese Academy of Sciences, Beijing 100190, China

[c] School of Environmental and Chemical Engineering, Jiangsu University of Science and Technology, Zhenjiang, Jiangsu 212003, China

[d] Advanced Light Source, Lawrence Berkeley National Laboratory, Berkeley CA 94720, USA

Supporting Information

Table of Contents

S1. A Computational Screening of Molecular Chromophores

The HOMO and LUMO energies, as well as HOMO-LUMO gaps of a series of molecular chromophores (Scheme S1) were evaluated computationally using the density functional theory (DFT). Calculations were performed with Guassian 09 suite of programs.[1] The geometries of selected chromophores were optimized with the hybrid functional B3LYP[2-4] and basis set DGDZVP[5, 6]. A frequency calculation was conducted at the end of each geometry optimization to ensure a true minimum.

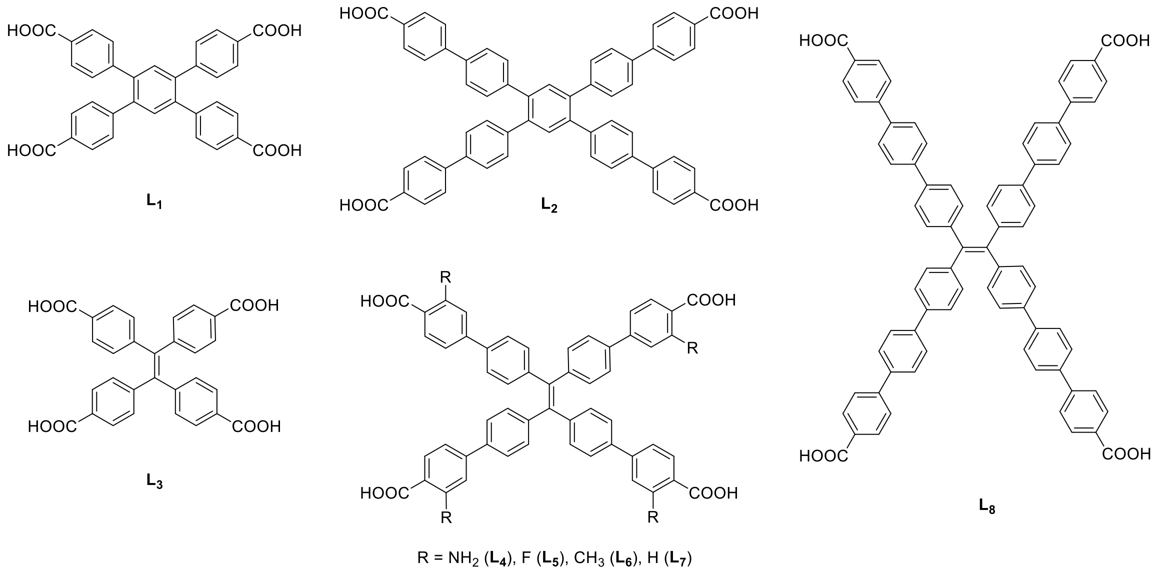

Scheme S1. Structures of selected molecular chromophores. L_1 = 4',5'-bis(4-carboxyphenyl)-[1,1':2',1''-terphenyl]-4,4''-dicarboxylic acid; L_2 = 4'',5''-di(4'-carboxy-[1,1'-biphenyl]-4-yl)-1,1':4',1'':2'',1''':4''',1''''-quinquephenyl-4,4''''-dicarboxylic acid; L_3 = tetrakis(4-carboxyphenyl)ethylene; L_4 = 4',4''',4''''',4'''''''-(ethene-1,1,2,2-tetrayl)tetrakis(3-amino-[1,1'-biphenyl]-4-carboxylic acid); L_5 = tetramethyl 4',4''',4''''',4'''''''-(ethene-1,1,2,2-tetrayl)tetrakis(3-fluoro-[1,1'-biphenyl]-4-carboxylate); L_6 = 4',4''',4''''',4'''''''-(ethene-1,1,2,2-tetrayl)tetrakis(3-methyl-[1,1'-biphenyl]-4-carboxylic acid); L_7 = 4',4''',4''''',4'''''''-(ethene-1,1,2,2-tetrayl)tetrakis([1,1'-biphenyl]-4-carboxylic acid); L_8 = 4'',4''''',4'''''''',4'''''''''''-(ethene-1,1,2,2-tetrayl)tetrakis([1,1':4',1''-terphenyl]-4-carboxylic acid).

Table S1. The calculated HOMO and LUMO energies along with the HOMO-LUMO gaps of chosen chromophores. ΔE_{cor} is normalized to the experimental value of L_7.

Method	B3LYP			Corrected
Basis Set	DGDZVP			
Ligand	HOMO (eV)	LUMO (eV)	ΔE (eV)	ΔE_{cor} (eV)
L_1	-6.66	-2.45	4.21	3.15
L_2	-6.17	-2.29	3.88	2.90
L_3	-6.40	-2.68	3.72	2.78

L_4	-5.70	-2.25	3.46	2.58
L_5	-6.10	-2.68	3.42	2.56
L_6	-5.80	-2.39	3.41	2.55
L_7	-5.87	-2.46	3.41	2.55
L_8	-5.65	-2.31	3.34	2.50

S2. The Synthesis of H_4tcbpe

The general synthesis of tpe-based ligand can be found in Scheme S2. The starting material, tpe-Br, is synthesized according to a reported method.[7] The detailed synthesis procedure for H_4tcbpe, as part of a US provisional patent filed on April 25, 2014, is listed below.[8] During the preparation of this manuscript, we found Zhou and coworkers also reported the synthesis of H_4tcbpe using a different procedure.[9]

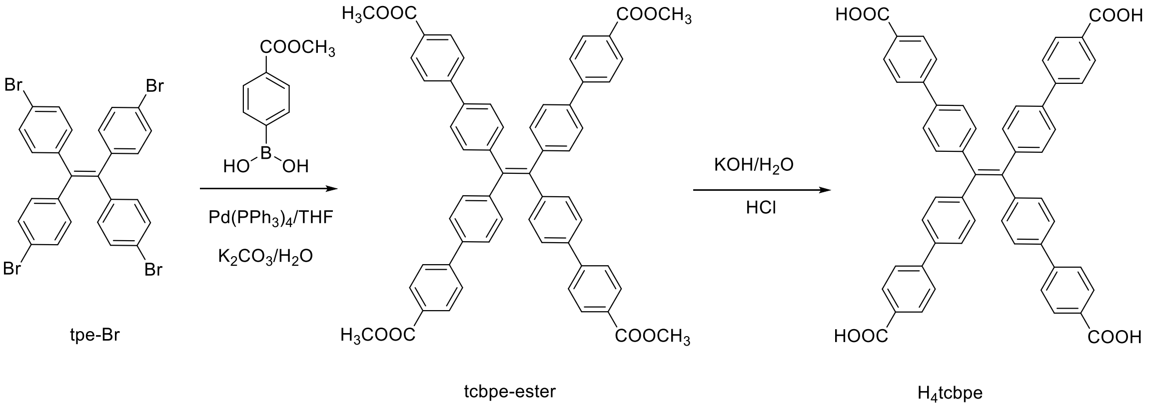

Scheme S2. The synthesis of H_4tcbpe

As shown in Scheme 2, tetra-(4-bromo-phenyl)ethylene (**tpe-Br**, 2.85 g, 4.4 mmol), 4-(methoxycarbonyl)phenylboronic acid (5.00 g, 27.8 mmol) and $Pd(PPh_3)_4$ (0.20 g, 0.2 mmol) were added into a 250 mL three-neck flask, then THF (tetrahydrofuran, 100 mL) and K_2CO_3 aqueous solution(3.0 M, 15 mL) were added under nitrogen protection at room temperature, and the mixture solution was kept at 90 ^{o}C for 3 days. After cooling to room temperature, the reaction solution was extracted with dichloromethane three times. The organic phase was washed with water, dried with anhydrous magnesium sulfate and then subject to flash chromatography using dichloromethane as the effluent. The product **tcbpe-ester** was obtained as green-yellow solid in 63.6% yield (2.43 g). ^{1}H NMR (400 MHz, $CDCl_3$) δ 8.07 (d, 8H, J = 8.1Hz), 7.64(d, 8H, J = 8.0Hz), 7.45(d, 8H, J = 7.9Hz), 7.21(d, 8H, J = 8.0Hz), 3.93(s, 12H); ^{13}C NMR (100 MHz, $CDCl_3$) δ 167.1, 145.0, 143.6, 140.8, 138.2, 132.2, 130.2, 129.0, 126.9, 52.3; MS (EI): calcd. for $C_{58}H_{44}O_8$: 868.3036; Found, 868 (M^+). Anal. Calcd for $C_{58}H_{44}O_8$: C, 80.17%; H, 5.10%. Found: C, 79.81%; H, 5.37%.

The **tcbpe-ester** (2.43 g, 2.8 mmol) was dissolved in THF (30 mL) and then conc. KOH solution (3M, 30 mL) was added. The mixture was refluxed for more than 4 h. After the reaction completed, the solution was cooled to room temperature and concentrated under reduced pressure. The concentrated solution was acidified with conc. HCl to form precipitates. The mixture was cooled and vacuum filtered, and the precipitate was washed with water and dried. The product **H_4tcbpe** was obtained as yellow powder in 90.5% yield (2.06 g). ^{1}H NMR (400 MHz, DMSO-d6) δ 12.96, 7.97 (d, 8H, J = 7.7Hz), 7.77 (d, 8H, J = 7.7 Hz), 7.62 (d, 8H, J = 7.6Hz), 7.20 (d, 8H, J = 7.6Hz); ^{13}C NMR (100 MHz, DMSO-d6) δ 167.1, 143.4, 143.1, 140.2, 137.1, 131.6, 129.9, 129.6, 126.5; MS (MALDI-TOF): calcd. for $C_{54}H_{36}O_8$: 812.2410; Found, 812.7 (M $^+$). Anal. Calcd for $C_{54}H_{36}O_8$: C, 79.79%; H, 4.46%. Found: C, 79.91%; H, 4.38%.

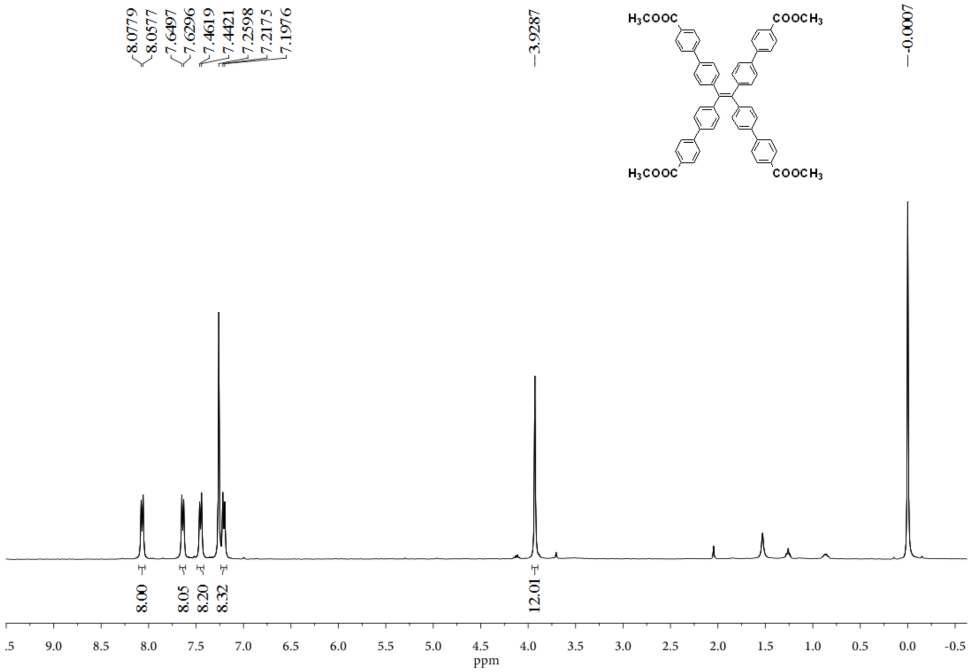

Figure S1. ^{1}H NMR of tcbpe-ester.

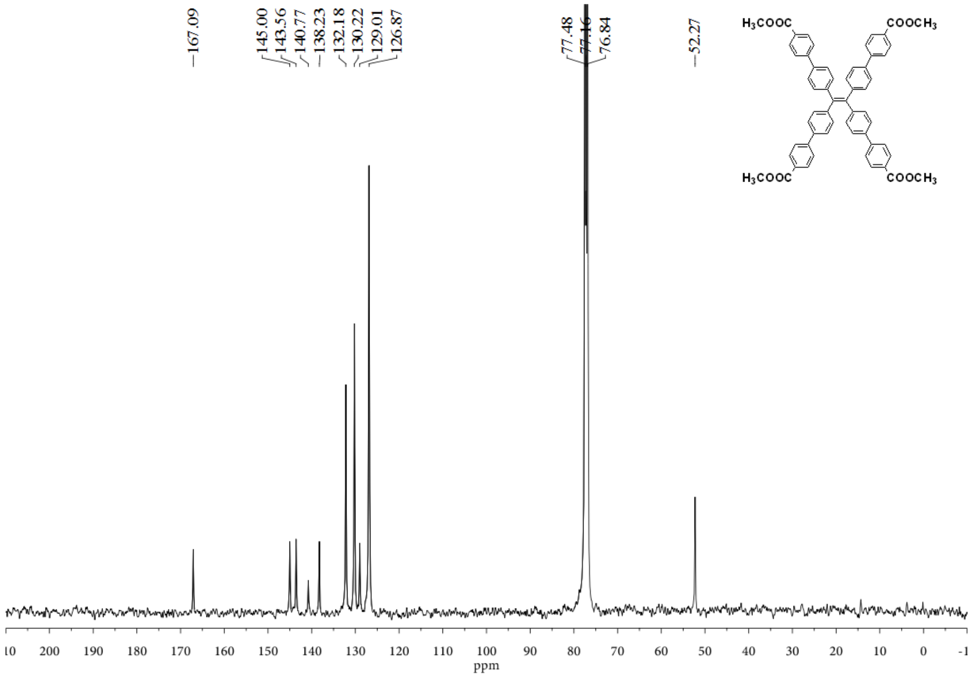

Figure S2. ^{13}C NMR of tcbpe-ester.

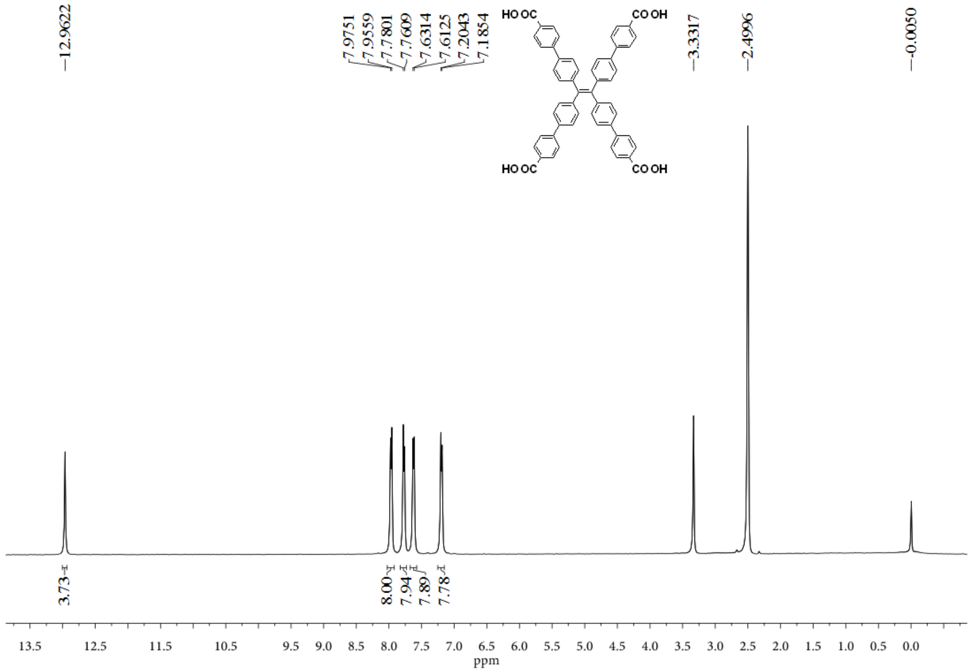

Figure S3. ^{1}H NMR of H_4tcbpe.

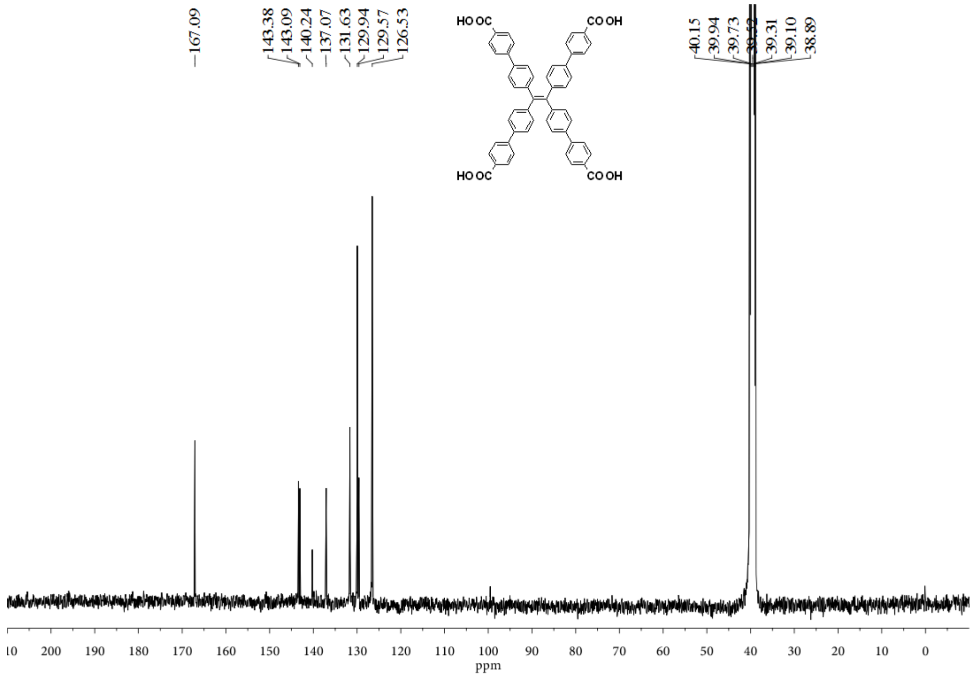

Figure S4. ^{13}C NMR of H_4tcbpe.

S3. The synthesis of Zn_2(tcbpe)·*x*DMA (LMOF-231)

$Zn(NO_3)_2 \cdot 6H_2O$ (0.0892 g, 0.30 mmol), H_4tcbpe (0.0244 g, 0.03 mmol), and N,N'-dimethylacetamide (DMA, 2 mL) were added in a 20 mL glass vial. The glass vial was capped and sonicated at room temperature for three minutes until a clear solution was obtained. The sealed glass vial was kept at 120 °C for 48 hours. Transparent light yellow single crystals were harvested through filtration, washed with DMA, and dried in air (~80% yield based on H_4tcbpe).

S4. Power X-ray Diffraction (PXRD) and Thermogravimetric Analysis (TGA)

PXRD patterns were collected on a Rigaku Ultima-IV diffractometer between 3° and 50° (2θ). TG experiments were performed on a TA Q5000IR analyzer. The thermal decomposition profile was acquired by heating a sample from room temperature to 600° under nitrogen flow (20 mL/min).

S5. Single Crystal X-ray Diffraction Analysis

Single crystal of H_4tcbpe was obtained by slow diffusion of diethyl ether vapor into the solution of H_4tcbpe in DMF/dioxane (v/v 1:1) at room temperature. All diffraction data were collected on a Rigaku Saturn X-ray diffractometer with graphite-monochromator Mo-Kα radiation (λ = 0.71073 Å) at 113 K. Intensities were corrected for absorption effects using the multi-scan technique SADABS. The structure was solved by direction methods and refined by a full matrix least squares technique based on F^2 using SHELXL 97 program[10]. The SQUEEZE routine within the crystallographic program PLATON[11] was employed in the treatment of the disordered solvent molecules of the crystal.

Synchrotron X-ray sources at the Advanced Light Source 11.3.1 Chemical Crystallography beam line were used to collect low temperature (100 K) single crystal diffraction data for LMOF-231. Reflection data for compound 1 were collected using a three-circle Bruker D8 diffractometer equipped with an APEXII detector (λ = 0.77490 Å) with 180 ω scans, at 0.3 steps, with settings of φ = 0, 120, and 240. The crystals were twinned. Using Cell_now[12], two orientation matrices were determined; the relationship between these components was determined to be 180 degrees about real axis [100]. The data were integrated using the two matrices in SAINT.[13] TWINABS[14] was used to produce a merged HKLF4 file for structure solution and initial refinement, and HKLF5 file for final structure refinement. The HKLF5 file contained the merged reflections first component and those that overlapped with this component, which were split into 2 reflections. TWINABS indicated the twin faction to be 53:47. The structure was solved using the HKLF4 file, but the best refinement was given by the HKLF5 file. All atoms were refined anisotropically. Hydrogens were placed in calculated position and refined using a riding model. The solvent was disordered and so the SQUEEZE routine in PLATON[11] was used to generate and solvent mask. The solvent molecules were not added to the chemical formula.

Table S2. Single crystal data for H_4tcbpe at 113 K

Compound	H_4tcbpe·2DMF
Formula	$C_{60}H_{50}N_2O_{10}$
M	959.02
Crystal system	Orthorhombic
Space group	Fdd2
a/Å	20.642(12)
b/Å	78.16(5)
c/Å	8.624(5)
α/o	90.00
β/o	90.00
γ/o	90.00
V, Å^3	13914(14)
Z	8
Temperature (K)	113(2)
λ (radiation wavelength) Å	0.71075
D, g/cm^3	0.916
Reflections collected	7394

R1[a] $[I > 2\sigma(I)]$	0.0971
wR2[b] $[I > 2\sigma(I)]$	0.2908
Goodness-of-fit	1.067
CCDC No.	908787 (submitted November 1, 2012)

[a] $R1 = \sum|F_o - F_c| / \sum|F_o|$
[b] $wR2 = \sum[w(F_o^2 - F_c^2)^2] / w(F_o^2)^2]^{1/2}$

Table S3. Single crystal data for LMOF-231 at 100 K

Compound	Zn_2(tcbpe)·*x*DMA (LMOF-231)
Formula	$C_{54}H_{32}O_8Zn_2$
M	939.53
Crystal system	Monoclinic
Space group	C 2/c
a/Å	36.929(5)
b/Å	31.080(4)
c/Å	11.8533(17)
α/o	90.00
β/o	99.228(2)
γ/o	90.00
V, $Å^3$	13429(3)
Z	8
Temperature (K)	100(2)
λ (radiation wavelength) Å	0.7749
D, g/cm^3	0.929
Reflections collected	76786
R1[a] $[I > 2\sigma(I)]$	0.0898
wR2[b] $[I > 2\sigma(I)]$	0.2803
Goodness-of-fit	1.058
CCDC No.	1004908

[a] $R1 = \sum|F_o - F_c| / \sum|F_o|$
[b] $wR2 = \sum[w(F_o^2 - F_c^2)^2] / w(F_o^2)^2]^{1/2}$

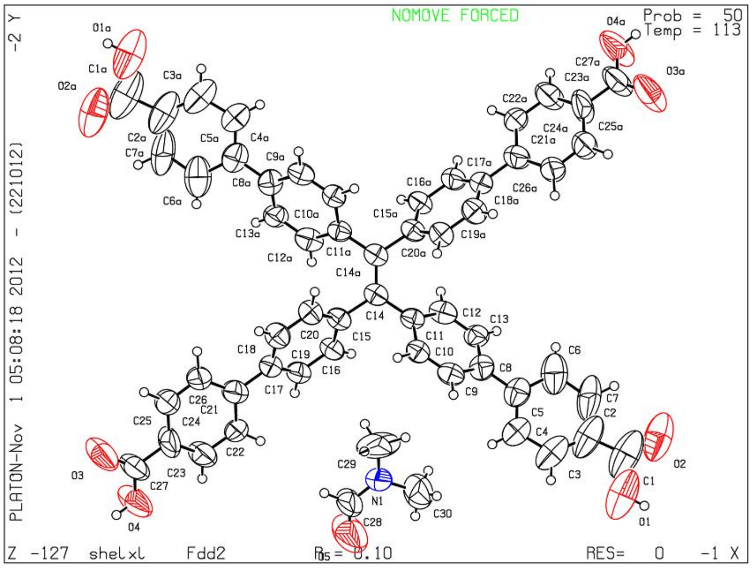

Figure S5. The ORTEP diagram of H_4tcbpe (thermal ellipsoids drawn in 50% probability).

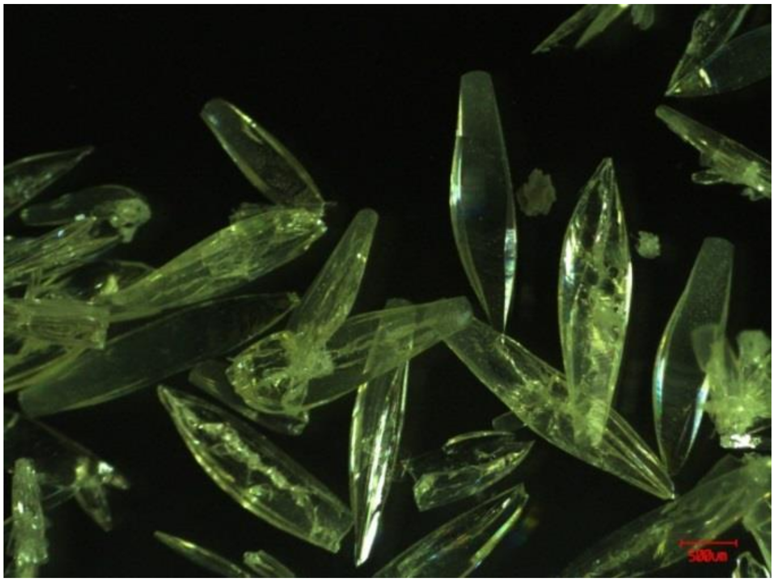

Figure S6. Crystals of LMOF-231 under a microscope.

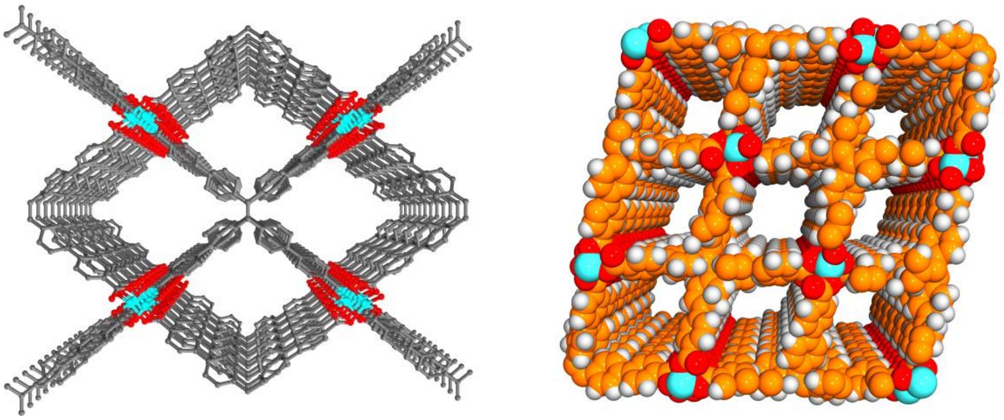

Figure S7. The overall 3D structure of LMOF-231 represented by a ball-and-stick model (left, H is omitted for clarity, C in grey, O in red, Zn in aqua) and a space-filling model (right, H in white, C in orange, O in red, Zn in aqua).

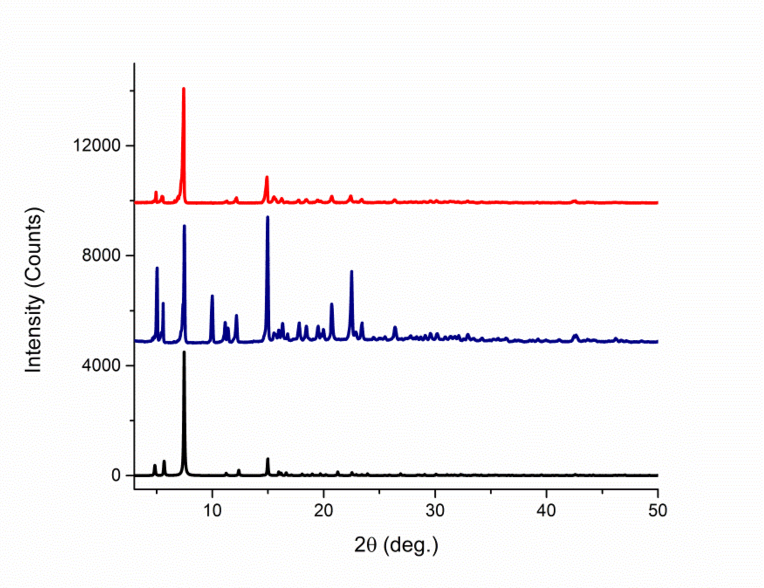

Figure S8. PXRD patterns of actived sample LMOF-231’ (top), as-made sample LMOF-231 (middle), and simulated pattern from the single crystal data (bottom).

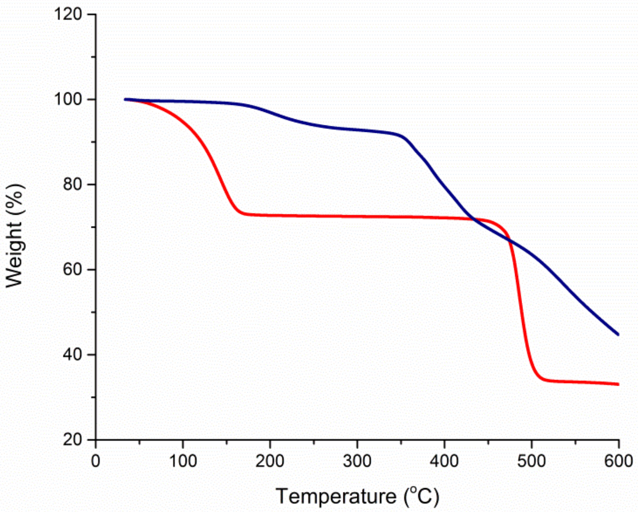

Figure S9. Thermogravimetric (TG) profile of H_4tcbpe (blue) and LMOF-231 (red) under nitrogen flow.

S6. Pore Charaterization

Gas sorption measurements were carried out on a volumetric gas sorption analyzer (Autosorb-1 MP, Quantachrome Instruments). Ultra high purity N2 (99.999%) was used for the experiment. Cryogenic temperature (77K) was achieved by using liquid nitrogen as coolant. About 120 mg as made sample was outgassed at 423 K overnight under dynamic vacuum and the subsequent degassed sample was used for the gas sorption experiment. The N2 isotherm was collected in a pressure range from 10^{-7} to 1 atm at 77K. Surface area was analyzed using Autosorbv1.50 software. The BET surface are for LMOF-231' (the ourgassed LMOF-231) is 833 m^2/g.

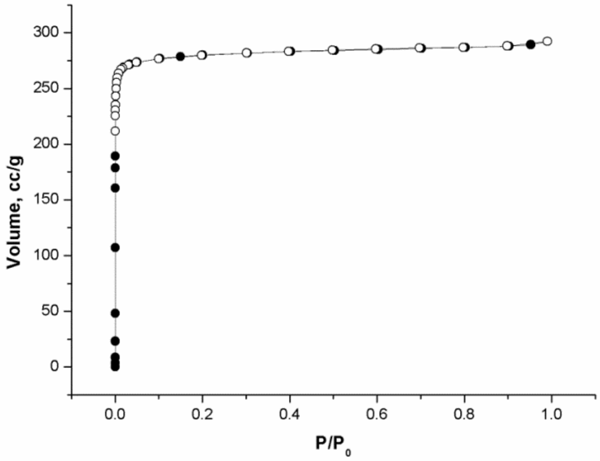

Figure S10. Nitrogen absorption curve (filled circle) and desorption curve (empty circle) of LMOF-231' at 77 K.

S7. Optical Absorption and Fluorescence Spectroscopy

The diffuse reflectance of solid samples were collected on a Shimadzu UV-3600 spectrophotometer at room temperature with a $BaSO_4$ standard as the baseline. The diffuse reflectance was converted to the Kubelka-Munk Function. The photoluminsecence (PL) study was conducted on a Varian Cary Eclipse spectrophotometer. Measurements were taken on solid samples at room temperature.

Activated sample LMOF-231' was sandwiched in between two pieces of Teflon sheets (American Durafilm) and the edges were sealed. This Teflon@LMOF assembly was kept at elevated temperatures for 12 hours. Fluorescence spectra were recorded before and after heating to evaluated the thermal stability of the LMOF.

Solvent-exchanged samples were prepared by immersing crystals of LMOF-231 in selected solvents. Solvents were decanted and fresh solvents were replenished every serveral hours for three days. Then solids were then collected and air-dried. Fluorescence spectra were taken on fresh solvent-exchanged samples to evaluated the solvent effect on emission maxima.

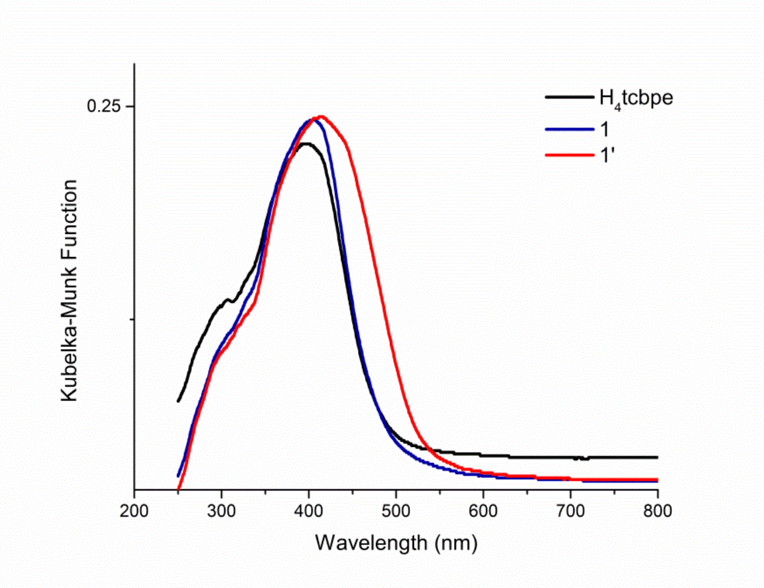

(a)

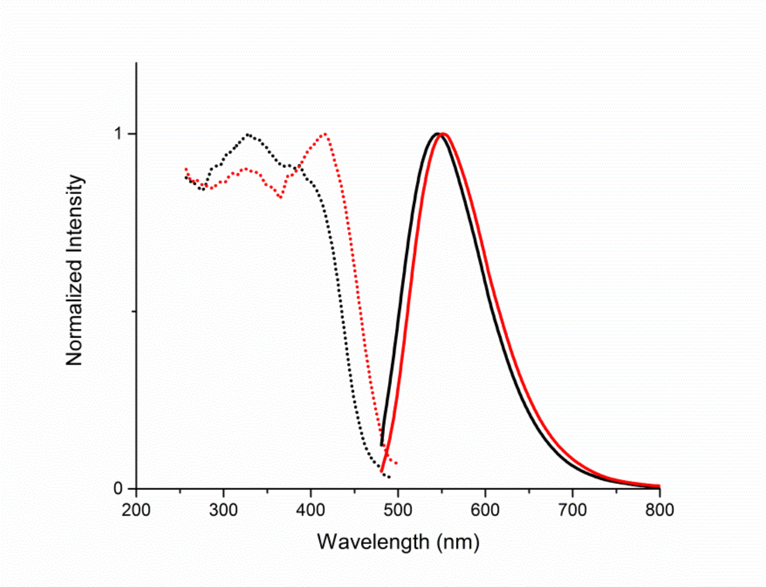

(b)

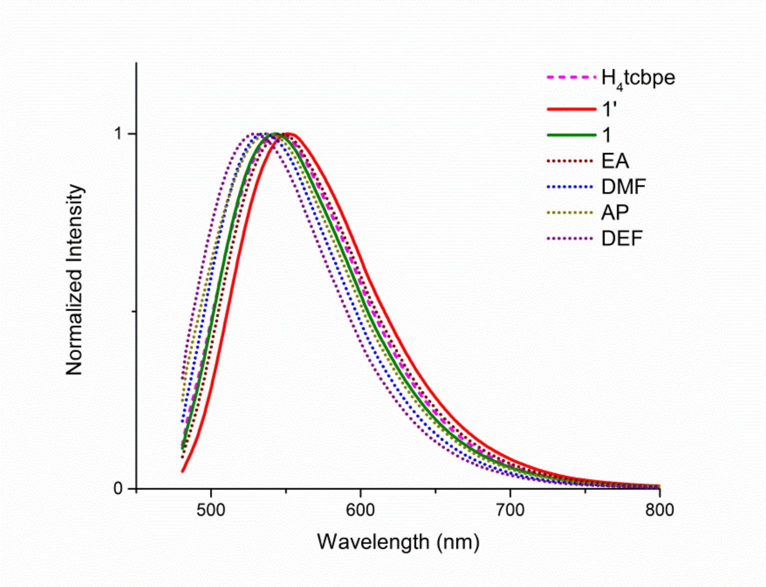

(c)

Figure S11. (a) Optical absorption spectra of H$_4$tcbpe, **1**, and **1’**. (b) Excitation spectra of H$_4$tcbpe (black dotted) and LMOF-231’ (red dotted). Emission spectra of H$_4$tcbpe (black solid) and LMOF-231’ (red solid) at λ_{ex} = 455 nm. (c) Emission spectra of H$_4$tcbpe, **1’,** and solvent exchanged LMOFs. Solvent abbreviation: ethyl acetate (EA), N,N-dimethylformamide (DMF), acetophenone (AP), N,N-diethylformamide (DEF). All emission spectra were acquired with λ_{ex} = 455 nm.

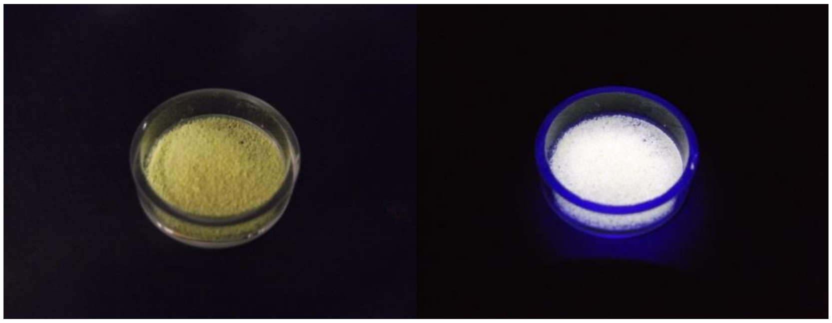

(a)

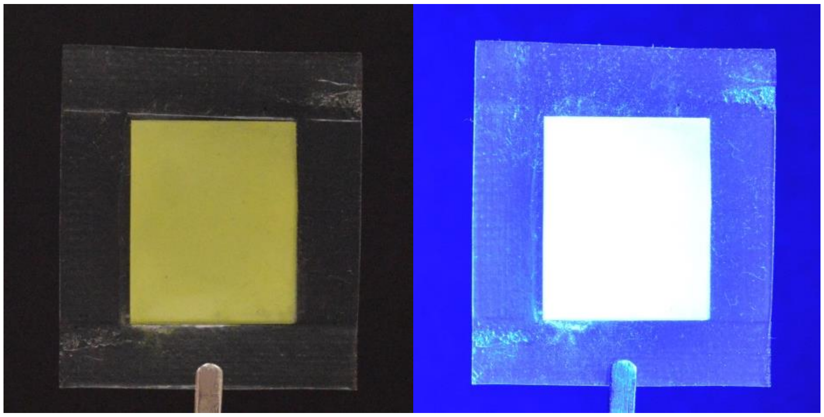

(b)

Figure S12. Photos of (a) LMOF-231’ under ambient light (left) and blue light (λ = 455 nm, right). (b) Teflon protected sample under ambient light (left) and blue light (λ = 450-470 nm, LED lamp, right)

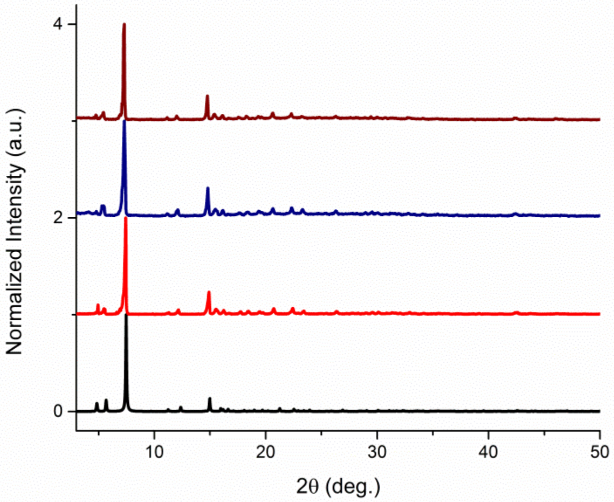

Figure S13. PXRD patterns (from bottom to top) of simulated LMOF-231 (black), fresh LMOF-231' (red), Telfon protected LMOF-231' after heating at 120°C (blue), and 150 °C (burgundy) for 12 hours.

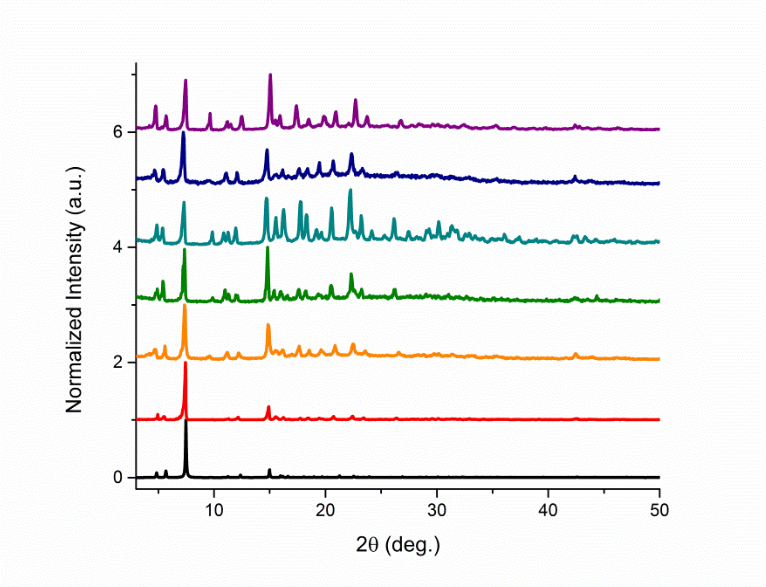

Figure S14. PXRD paterns (from bottom to top) of simulated LMOF-231 (black), LMOF-231' (red), LMOF samples exchanged in ethyl acetate (EA, orange), N,N-dimethylacetamide (DMA, or as-made, green), acetophenone (AP, cyan), N,N-dimethylformamide (DMF, blue), N,N-diethylformamide (DEF, purple).

S8. Quantum Yield and Luminous Efficacy

The internal quantum yields of ligand and LMOFs were measured on a Hamamatsu C9220-03 system with a 150 W xenon monchromatic lamp and an integrating sphere. The external quantum yields were measured on a QE-2000 system with a 150 W xenon lamp and an integrating hemisphere by Otsuka Electronics Co. Ltd. Solids samples were used for all measurements.

Table S4. Photophysical properties of H_4tcbpe and compound **1**.

Internal Quantum Yield (%)				
Sample	λ_{ex} = 420 nm	λ_{ex} = 440 nm	λ_{ex} = 455 nm	λ_{em} (nm) [b]
H_4tcbpe	70.3±0.1	63.2±0.1	62.3±0.1	540
1'	95.1±0.2	81.3±0.1	76.4±0.2	550
TF@**1**' [a]	92.2±0.1 [c]	80.9±0.1	73.2±0.1	550
1'·DMA (**1**)	82.5±0.1	74.7±0.1	72.2±0.1	540
1'·DMF	92.4±0.1	73.6±0.1	73.7±0.1	535
1'·DEF	81.0±0.1	71.7±0.1	71.5±0.1	530

1’·EA	93.9±0.1	81.1±0.6	76.3±0.1		545
1’·AP	72.1±0.1	68.0±0.1	60.3±0.1		540
External Quantum Yield (expressed as % of Internal Quantum Yield)					
Sample	λ_{ex} = 400 nm	λ_{ex} = 415 nm	λ_{ex} = 440 nm	λ_{ex} = 455 nm	λ_{em} (nm) [b]
1	96.0	94.2	80.6	64.6	540
1’	96.5	96.0	93.3	88.7	550
Thermal stability [d] (Decrease in Percent Intensity, ±2%)					
Sample	100 °C	120 °C	150 °C	160 °C	λ_{em} (nm) [b]
TF@**1**’	1	2	10	15	550

[a] Teflon protected sample in 120 °C oven for 12 h. [b] λ_{ex} = 455 nm. λ_{em} has a ±2nm deviation. [c] λ_{ex} = 415 nm [d] Sample under different temperatures for 12 h, λ_{ex} = 455 nm.

Fine powder of LMOF-231’ was dispersed in ethyl acetate under ultrasonication for 1 hour. A LED bulb was then dipped in this suspension and air dried. This process was repeated a few times until a uniform phosphor layer was deposited. Alternatively, this phosphor can be coated by spraying the suspension onto the targeted surface.

The lunimous efficacy of a PC-WLED assembly (a 5 mm, 20 mA, 3 V, 455-460 nm LED bulb coated with LMOF-231’) was evaluated on a MCPD-9800(3683) P16 system with a halfmoon integrating sphere (HM500 base-down) by Otsuka Electronics Co. Ltd. A total of 180 measurements were performed, and the average value was reported.

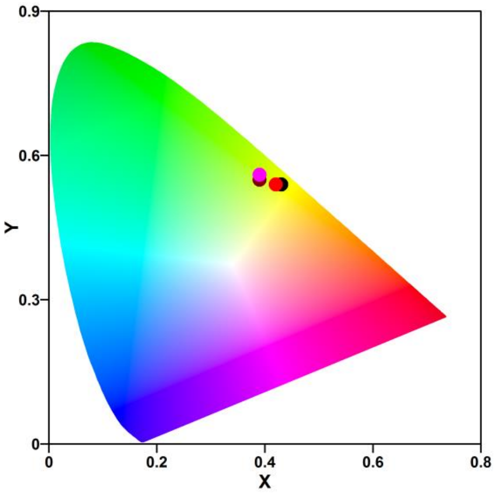

Figure S15. CIE coordionates of YAG:Ce^{3+}, black dot, (0.43, 0.54), H_4tcbpe, burgundy dot, (0.39, 0.55), LMOF-231, pink dot, (0.39, 0.56), and LMOF-231’, red dot, (0.42, 0.54) calculated from their emission spectra respectively (λ_{ex} = 455 nm).

S9. References

1. M. J. Frisch, G. W. Trucks, H. B. Schlegel, G. E. Scuseria, M. A. Robb, J. R. Cheeseman, G. Scalmani, V. Barone, B. Mennucci, G. A. Petersson, H. Nakatsuji, M. Caricato, X. Li, H. P. Hratchian, A. F. Izmaylov, J. Bloino, G. Zheng, J. L. Sonnenberg, M. Hada, M. Ehara, K. Toyota, R. Fukuda, J. Hasegawa, M. Ishida, T. Nakajima, Y. Honda, O. Kitao, H. Nakai, T. Vreven, J. J. A. Montgomery, J. E. Peralta, F. Ogliaro, M. Bearpark, J. J. Heyd, E. Brothers, K. N. Kudin, V. N. Staroverov, T. Keith, R. Kobayashi, J. Normand, K. Raghavachari, A. Rendell, J. C. Burant, S. S. Iyengar, J. Tomasi, M. Cossi, N. Rega, J. M. Millam, M. Klene, J. E. Knox, J. B. Cross, V. Bakken, C. Adamo, J. Jaramillo, R. Gomperts, R. E. Stratmann, O. Yazyev, A. J. Austin, R. Cammi, C. Pomelli, J. W. Ochterski, R. L. Martin, K. Morokuma, V. G. Zakrzewski, G. A. Voth, P. Salvador, J. J. Dannenberg, S. Dapprich, A. D. Daniels, O. Farkas, J. B. Foresman, J. V. Ortiz, J. Cioslowski and D. J. Fox, Gaussian 09, Revision C.01, Gaussian, Inc., Wallingford CT, 2010.
2. A. D. Becke, *Phys. Rev. A*, 1988, **38**, 3098-3100.
3. C. Lee, W. Yang and R. G. Parr, *Phys. Rev. B*, 1988, **37**, 785-789.
4. A. D. Becke, *J. Chem. Phys.*, 1993, **98**, 5648-5652.
5. N. Godbout, D. R. Salahub, J. Andzelm and E. Wimmer, *Can. J. Chem.*, 1992, **70**, 560-571.
6. C. Sosa, J. Andzelm, B. C. Elkin, E. Wimmer, K. D. Dobbs and D. A. Dixon, *J. Phys. Chem.*, 1992, **96**, 6630-6636.
7. V. S. Vyas, M. Banerjee and R. Rathore, *Tetrahedron Lett.*, 2009, **50**, 6159-6162.
8. J. Li, Z. Hu and Q. Gong, 4/25/2014, US Provisional 61984154.
9. Z. Wei, Z.-Y. Gu, R. K. Arvapally, Y.-P. Chen, R. N. McDougald, J. F. Ivy, A. A. Yakovenko, D. Feng, M. A. Omary and H.-C. Zhou, *J. Am. Chem. Soc.*, 2014, **136**, 8269-8276.
10. G. M. Sheldrick, SHELX-97, Program for Structure Refinement, University of Göettingen, Germany, 1997.
11. A. L. Spek, PLATON, A multipurpose crystallographic tool ; Utrecht University: Utrecht, The Netherlands, 2001.
12. G. M. Sheldrick, *CELL_NOW, V. 2008/2. Bruker AXS, Inc., Madison, Wisconsin, USA*, 2008.
13. APEX II, *V. 2009.3-0, Bruker AXS, Inc., Madison, Wisconsin, USA*, 2009.
14. G. M. Sheldrick, *TWINABS, V. 2012/1, Bruker AXS Inc., Madison, Wisconsin, USA*, 2012.